

The 3D Galactocentric velocities of Kepler stars: marginalizing over missing RVs

RUTH ANGUS,^{1,2} ADRIAN M. PRICE-WHELAN,² DANIEL FOREMAN-MACKEY,² JOEL ZINN,³ AND MEGAN BEDELL²

¹*Department of Astrophysics, American Museum of Natural History, 200 Central Park West, Manhattan, NY, USA*

²*Center for Computational Astrophysics, Flatiron Institute, 162 5th Avenue, Manhattan, NY, USA*

³*NSF Fellow, Department of Astrophysics, American Museum of Natural History, 200 Central Park West, Manhattan, NY, USA*

ABSTRACT

Precise Gaia measurements of positions, parallaxes, and proper motions provide an opportunity to calculate 3D positions and 2D velocities (*i.e.* 5D phase-space) of Milky Way stars. Where available, spectroscopic radial velocity (RV) measurements provide full 6D phase-space information. Gaia will provide RVs for stars as faint as the 15th magnitude in its third data release, however there are now and will remain many stars without RV measurements. Without an RV it is not possible to directly calculate 3D stellar velocities, however it is still possible to *infer* 3D stellar velocities by marginalizing over the missing RV dimension. In this paper, we infer the 3D velocities of stars in the Kepler field in Cartesian Galactocentric coordinates (v_x , v_y , v_z). We directly calculate velocities for around a third of all Kepler targets, using RV measurements available from the Gaia, LAMOST and APOGEE spectroscopic surveys. Using the velocity distributions of these stars as our prior, we infer velocities for the remaining two-thirds of the sample by marginalizing over the RV dimension. The median uncertainties on our inferred v_x , v_y , and v_z velocities are around 5, 18, and 4 kms^{-1} , respectively. We provide 3D velocities for 185,223 stars in the Kepler field, with and without RV measurements. These 3D velocities will enable kinematic age-dating, Milky Way stellar population studies, and many other scientific studies that use the benchmark sample of well-studied Kepler stars. Although the methodology used here is broadly applicable to targets across the sky, our prior is specifically constructed from and for the Kepler field. Care should be taken to use a suitable prior when extending this method to other parts of the Galaxy.

Keywords: Milky Way Dynamics

1. INTRODUCTION

Gaia has revolutionized the field of Galactic dynamics by providing positions, parallaxes and proper motions with unparalleled precision, for a large number of Milky Way stars. So far, Gaia has provided positions, parallaxes and proper motions for around 1.7 billion stars, and radial velocities (RVs) for more than 7 million stars across its 1st, 2nd and early-3rd data releases (Gaia Collaboration et al. 2016, 2018, 2020). In combination, proper motion, position, and RV measurements provide full 6D phase-space information for any given star, which can be used to calculate its Galactic orbit. The orbits of stars are useful for kinematic age-dating, for exploring the secular dynamical evolution of the Galaxy, for differentiating between nascent and accreted stellar populations in the Milky Way’s halo, and many other applications.

Our main motivation for calculating the velocities of Kepler targets is to use Galactic kinematics to study stellar evolution, either by using vertical velocity dispersion as an age proxy, or by calculating stellar ages via an age-velocity dispersion relation (*e.g.* Angus et al. 2020; Lu et al. 2021). The ages of stars, particularly GKM stars on the main sequence, are difficult to measure because their luminosities and temperatures evolve slowly (see Soderblom 2010, for a review of stellar ages). Galactic kinematics provides an alternative, statistical dating method.

The star forming molecular gas clouds observed in the Milky Way have a low out-of-plane, or vertical, velocity (*e.g.* Stark & Brand 1989; Stark & Lee 2005; Aumer & Binney 2009; Martig et al. 2014; Aumer et al. 2016). In contrast, the vertical velocities of older stars are observed to be larger in magnitude on average (Strömberg 1946; Wielen 1977; Nordström et al. 2004; Holmberg et al. 2007, 2009; Aumer & Binney 2009; Casagrande et al. 2011; Yu & Liu 2018; Ting & Rix 2019). Galaxy formation simulations indicate that stars initially form from dynamically hot gas, which

settles into a cooler thin disk over time during the early stages of Galactic evolution (*e.g.* Bird et al. 2013). After this initial cooling phase, giant molecular clouds and Galactic spiral arms dynamically ‘reheat’ the orbits of stars over time. Regardless of the exact history of dynamical cooling and heating, older populations of stars are observed to have larger velocity dispersions than younger populations. This behavior is codified by empirically-calibrated Age-Velocity dispersion Relations (AVRs), which typically express the relationship between age and velocity dispersion as a power law: $\sigma_v \propto t^\beta$, with free parameter, β (*e.g.* Holmberg et al. 2009; Yu & Liu 2018; Mackereth et al. 2019). These expressions can be used to calculate the ages of stellar populations from their velocity dispersions. However, AVRs are usually calibrated in 3D Galactocentric velocities, and most commonly in vertical velocity: v_z or W . Regardless of the coordinate system, some transformation from RV and proper motion in equatorial coordinates is usually required to calculate the kinematic ages of stars using an AVR.

RV measurements, combined with positions, parallaxes, and proper motions measured in the plane of the sky, complete the full set of information needed to calculate 3D stellar velocities. However, RV can only be measured from a stellar spectrum – an observation that requires a significant number of photons and is thus expensive to obtain, particularly for faint stars. Fortunately however, Gaia proper motion measurements are of such incredible precision that, even without an RV measurement, the 3D velocity of a star can still be inferred by marginalizing over radial velocity. This will often provide a velocity that is not equally well-constrained in every direction, *i.e.* the probability density function of a star’s velocity will be an oblate spheroid in 3D. In the equatorial coordinate system, a star’s velocity will be tightly constrained in the directions of RA and dec, and only constrained by the prior in the radial direction. Transforming to any other coordinate system, a star’s velocity probability density function will change shape via a transformation that depends on its position.

In this work, we provide 3D velocities in v_x , v_y , and v_z for Kepler targets. Our motivation is chiefly to calculate vertical velocities (v_z) which can then be used to calculate the ages of stellar populations via an AVR, from which other empirical age-dating methods can be calibrated. For example, empirical or semi-empirical models that relate the magnetic activity or rotation periods of stars to their age can be used to infer the ages of some low-mass dwarfs (*e.g.* Skumanich 1972; Barnes 2003, 2007; Mamajek & Hillenbrand 2008; Matt et al. 2012; Angus et al. 2019; Claytor et al. 2020), however, these empirical relations are often poorly calibrated for low-mass and old stars (*e.g.* Angus et al. 2015; van Saders et al. 2016, 2018; Metcalfe & Egeland 2019; Curtis et al. 2020; Spada & Lanzafame 2019; Angus et al. 2020). In Angus et al. (2020) we used the velocities of Kepler stars in the direction of Galactic latitude, v_b as a proxy for vertical velocity. v_b can be calculated without an RV and it is similar to v_z for many Kepler stars because the Kepler field lies at low Galactic latitude. We used the v_b velocity dispersions of stars as an age proxy to explore the evolution of stellar rotation rates. In Lu et al. (2021) we used *vertical* velocity dispersion (v_z) to calculate kinematic ages for Kepler stars with measured rotation periods using an age-velocity dispersion relation (AVR). Those vertical velocities were inferred by marginalizing over missing RVs using the method we describe in this paper. To expand upon that work and provide an opportunity to apply kinematic age-dating to more stars, we here calculate the 3D velocities of *all* Kepler targets. Although we focus on the Kepler field, the methodology presented in this paper is applicable to stars across the sky if a suitable prior is used.

There are several other applications for which the 3D velocity of a star is useful, even if its velocity is not equally well-constrained in every direction. For example, Oh et al. (2017) used Gaia proper motions to identify comoving pairs and groups of stars by marginalizing over missing RVs. In their study, the relative space motions of pairs of stars were used to establish whether they qualified as ‘comoving’. In a pathological case where two stars have near identical proper motions and completely different RVs, their method would incorrectly flag them as comoving stars, however in general the Gaia proper motion precision is sufficiently high to make these cases rare.

Another work that predicts 3D velocities of Gaia targets is Dropulic et al. (2021), in which the velocities of Gaia stars are predicted with a neural network. The network is trained on the velocities of stars *with* RVs and used to predict the velocities of stars without. The method we present here seeks to solve the same problem via a different methodology: we use Bayesian inference instead of machine learning. It is not possible to draw a direct comparison between their method and ours because we use different coordinate systems (we use Cartesian, and they use cylindrical coordinates), and because we focus on different populations – they predict velocities for the entire Gaia catalog, whereas we concentrate on a small part of the sky. The two approaches will be useful for different scientific applications, and it is extremely useful to have multiple approaches to solving this fundamental problem in astronomy.

This paper is laid out as follows. In section 2 we describe the data used in this paper. In section 3 we describe how we calculate the kinematic ages of Kepler stars from their positions, proper motions and parallaxes, marginalizing over

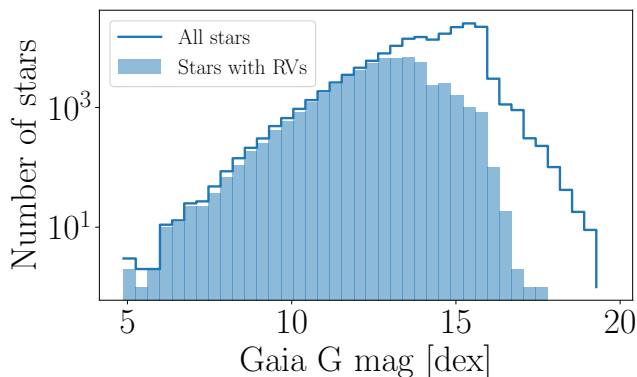
missing RVs. We also justify the choice of prior probability density function (PDF). In section 4 we present the 3D velocities of 185,223 Kepler stars and explore the accuracy and precision of our method.

2. THE DATA

We used the Kepler-Gaia cross-matched catalog available at gaia-kepler.fun, which contains 198,451 Kepler targets, cross-matched with Gaia targets within a $1''$ radius. This catalog includes Gaia positions, parallaxes, and proper motions from Gaia EDR3 and RVs from Gaia DR2. It also includes distances inferred from Gaia EDR3 parallaxes (Bailer-Jones et al. 2021). We crossmatched this catalog with the LAMOST DR5 catalog and the APOGEE DR16 stellar catalog also using a $1''$ radius (Cui et al. 2012; Ahumada et al. 2020; Xiang et al. 2019). We removed stars with a Gaia parallax < 0 , parallax signal-to-noise ratio < 10 , or Gaia astrometric excess noise > 5 . After applying these cuts our total number of targets was 185,223 stars: 29,512 with RVs from Gaia DR2, 38,581 from LAMOST DR5, and 21,267 from APOGEE DR16. In total, 58,270 stars in our sample have RVs from *either* Gaia, LAMOST, or APOGEE. The APOGEE survey has a higher spectral resolution than Gaia, which in turn is higher than LAMOST. The median RV uncertainty for stars in our sample is around 0.1 km/s for APOGEE RVs, 1 km/s for Gaia RVs, and 4 km/s for LAMOST RVs. In cases where stars had two or more available RV measurements, we adopted APOGEE RVs as a first priority, followed by Gaia, then LAMOST.

Although RVs are available for more than one in three Kepler targets, most stars with RV measurements are bright. Very few of the faintest stars have RVs because of the selection functions of spectroscopic surveys. Most of the stars in our sample with Gaia RV measurements are brighter than around 14th magnitude in Gaia G -band, and stars with LAMOST or APOGEE RVs are mostly brighter than around 16th magnitude. Figure 1 shows the apparent magnitude and temperature distributions of the stars in our sample, with and without RVs. This figure reveals the combined selection functions of the Gaia, LAMOST and APOGEE RV surveys and shows that faint stars are less likely to have RV measurements than bright ones.

Figure 1. The distribution of apparent Gaia magnitudes for stars in our sample with and without RV measurements from Gaia, LAMOST and APOGEE.

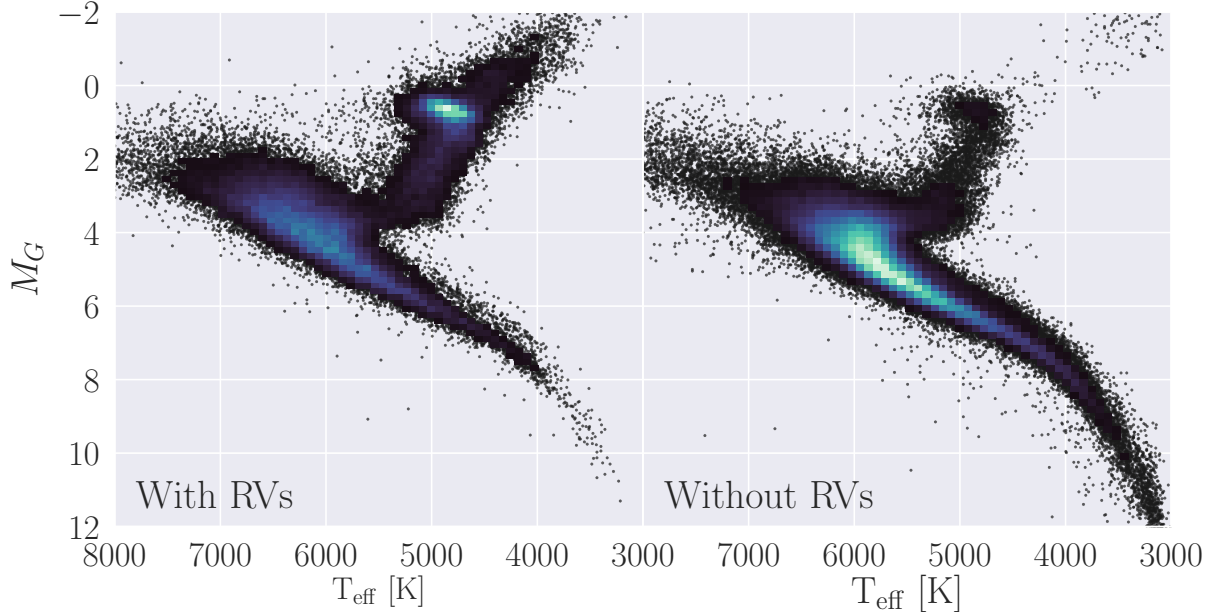


To illustrate how the populations of stars with and without RVs differ, we plot them on a color-magnitude diagram (CMD) in figure 2. The stars with RVs are generally hotter and more luminous than stars without. Most stars with RVs fall on the upper main sequence, the red giant branch, and the red clump. Most stars without RVs fall on the main sequence. This overall selection function is a combination of the APOGEE, LAMOST and Gaia DR2 selection functions.

3. METHOD

In this section we describe how we calculate full 3D velocities for stars in the Kepler field. Around 1 in 3 Kepler targets have an RV from either Gaia, LAMOST, or APOGEE. For these 58,270 stars we calculated 3D velocities using the `coordinates` library of `astropy` (Astropy Collaboration et al. 2013; Price-Whelan et al. 2018). This library performs a series of matrix rotations and translations to convert stellar positions and velocities in equatorial coordinates into positions and velocities in Galactocentric coordinates. It converts positions, proper motions, parallaxes/distances,

Figure 2. A magnitude-temperature diagram of stars in the Kepler field with (left) and without (right) RVs provided by Gaia, LAMOST and APOGEE. The stars with RVs are generally hotter and more luminous than those without RVs, and include a large number of red clump stars and red giant branch stars. Stars without RVs are mostly concentrated on the main sequence.



and RVs into \mathbf{x} , \mathbf{y} , \mathbf{z} , v_x , v_y , v_z . For stars *without* RVs, we inferred their velocities by marginalizing over their RVs using the method described below.

3.1. Inferring 3D velocities (marginalizing over missing RV measurements)

For each star in our sample without an RV measurement, we inferred v_x , v_y , and v_z from the 3D positions – RA (α), dec (δ), and parallax (π), and 2D proper motions (μ_α and μ_δ) provided in the *Gaia* EDR3 catalog (Gaia Collaboration et al. 2020). We also simultaneously inferred distance (instead of using inverse-parallax) to model velocities (see *e.g.* Bailer-Jones 2015; Bailer-Jones et al. 2018).

Using Bayes rule, the posterior probability of the velocity parameters given the Gaia data can be written:

$$p(\mathbf{v}_{\mathbf{xyz}}, D | \mu_\alpha, \mu_\delta, \alpha, \delta, \pi) = p(\mu_\alpha, \mu_\delta, \alpha, \delta, \pi | \mathbf{v}_{\mathbf{xyz}}, D) p(\mathbf{v}_{\mathbf{xyz}}) p(D), \quad (1)$$

where D is distance and $\mathbf{v}_{\mathbf{xyz}}$ is the 3D vector of velocities. To evaluate the likelihood function, our model predicts observable data from model parameters, *i.e.* it converts v_x , v_y , v_z and D to μ_α , μ_δ and π . In the first step of the model evaluation, cartesian coordinates, \mathbf{x} , \mathbf{y} , and \mathbf{z} are calculated from α , δ , and D by applying a series of matrix rotations, and a translation to account for the Solar position. The cartesian Galactocentric velocity parameters, v_x , v_y , and v_z , are then converted to equatorial coordinates, μ_α and μ_δ via another rotation. The posterior PDFs of the parameters v_x , v_y , v_z , and $\ln(D)$ are sampled by evaluating this model over a range of parameter values which are chosen by via the No U-Turns Sampler (NUTS) algorithm in PyMC3. At each set of model parameters the likelihood is calculated via a Gaussian likelihood function, and multiplied by a prior (described below) to produce the posterior probability: the probability of those model parameters given the data.

For computational efficiency, we used PyMC3 to sample the posterior PDFs of stellar velocities (Salvatier et al. 2016). This required that we rewrite the `astropy` coordinate transformation code using `numpy` and `Theano` (Harris et al. 2020; The Theano Development Team et al. 2016). The series of rotations and translations required to convert from equatorial to Galactocentric coordinates is described in the `astropy` documentation¹. For each star in the Kepler field,

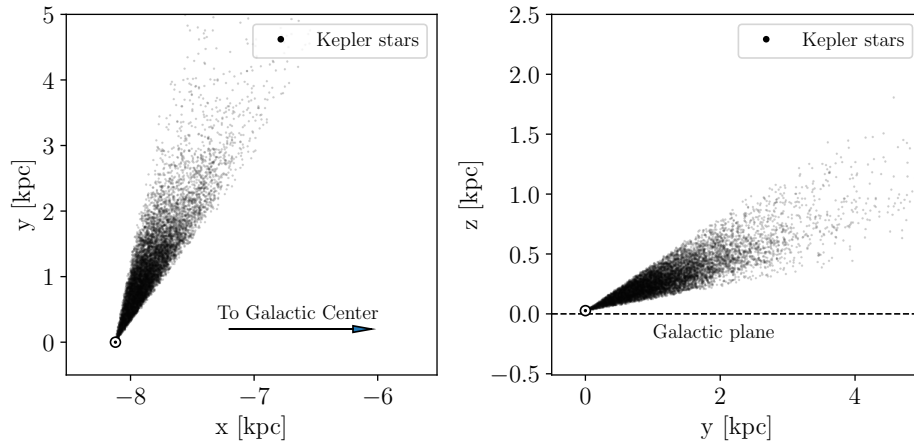
¹ <https://docs.astropy.org/en/stable/coordinates/galactocentric.html>

we explored the posteriors of the four parameters, v_x , v_y , v_z , and $\ln(D)$ using the *PyMC3* No U-Turn Sampler (NUTS) algorithm, and the *exoplanet* *Python* library (Foreman-Mackey & Barentsen 2019). We tuned the *PyMC3* sampler for 1500 steps, with a target acceptance fraction of 0.9, then ran four chains of 1000 steps for a total of 4000 steps. This resulted in a \hat{r} -statistic (the ratio of intra-chain to inter-chain variance) of around unity, indicating convergence. Using *PyMC3* made this inference procedure exceptionally fast – taking just a few seconds per star on a laptop.

3.2. The prior

As mentioned previously, the positioning of the Kepler field at low Galactic latitude allows v_z to be well-constrained from proper motion measurements alone. This also happens to be the case for v_x , because the direction of the Kepler field is almost aligned with the y -axis of the Galactocentric coordinate system and is almost perpendicular to both the x and z -axes (see figure 3). For this reason, the y -direction is similar to the radial direction for observers near the Sun, so v_y will be poorly constrained for Kepler stars without RV measurements. On the other hand, v_x and v_z are almost perpendicular to the radial direction and can be precisely inferred with proper motions alone.

Figure 3. x , y and z positions of stars observed by Kepler, showing the orientation of the Kepler field. The direction of the field is almost aligned with the y -axis and almost perpendicular to the x and z -axes, which is why v_x and v_z can be tightly constrained for Kepler stars without RVs, but v_y cannot.

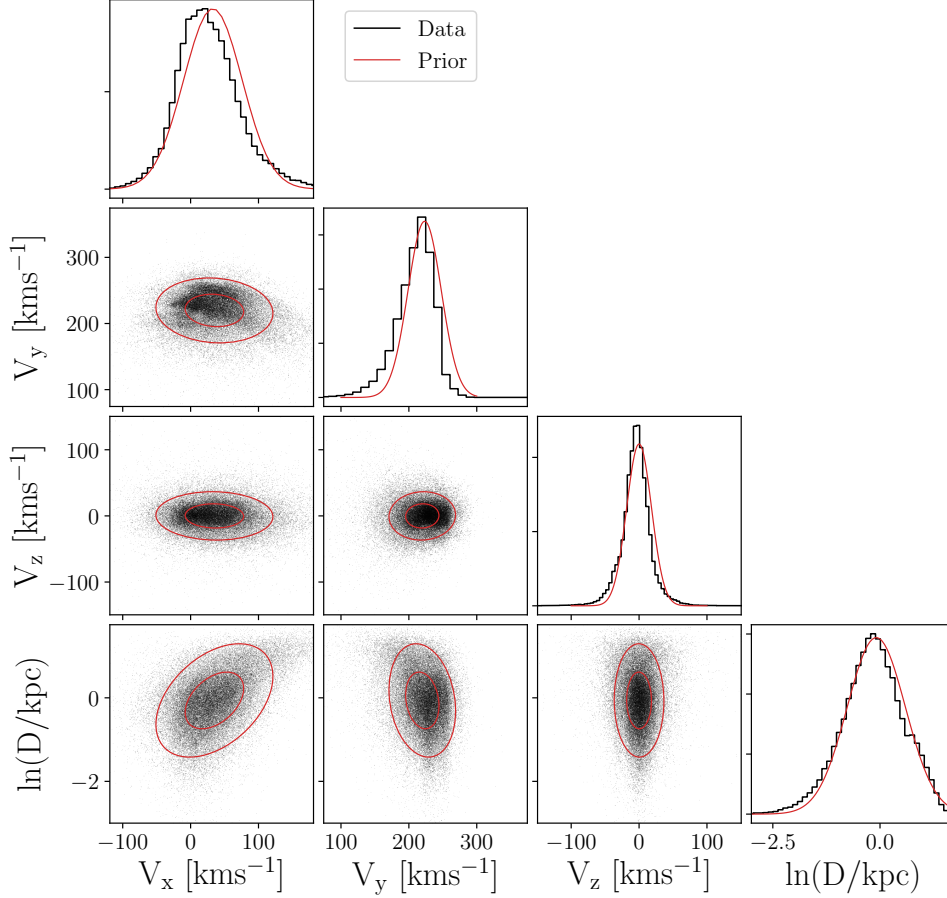


We constructed a multivariate Gaussian prior PDF over distance and 3D velocity using the Kepler targets *which have RV measurements*. We calculated the means and covariances of the v_x , v_y , v_z and $\ln(D)$ distributions of stars with measured RVs and then used these means and covariances to construct a multivariate Gaussian prior over the velocity and distance parameters for stars *without* RVs. Velocity and distance outliers greater than 3σ were removed before calculating the means and covariances of the distributions. The distance and velocity distributions of Kepler targets with RVs are displayed in figure 4. These are the distributions we used to construct the prior. The 1- and 2- σ contours of the multivariate Gaussian prior is shown in each panel in red.

Our goal was to infer the velocities of stars *without* RV measurements using a prior calculated from stars *with* RV measurements. However, stars with and without RVs are likely to be quite different populations, determined by the Gaia, LAMOST and APOGEE selection functions. In particular, stars without RV measurements are more likely to be fainter, less luminous, cooler and potentially older. Figure 2 shows the populations of stars with and without RVs on the CMD – stars with RVs are more likely to be upper-main-sequence and red giant stars, and stars without RVs are more likely to be mid and lower main-sequence dwarfs. For this reason, a prior based on the velocity distributions of stars *with* RVs will not necessarily reflect the velocities of those without.

We tested the influence of the prior on the velocities we inferred. One of the main features of the RV selection functions is brightness: Gaia DR2 RVs are only available for stars brighter than around 14th magnitude, and LAMOST DR5 and APOGEE DR16 RVs for stars brighter than around 16th magnitude. For this reason, we tested priors based on stellar populations with different apparent magnitudes. Three priors were tested: one calculated from the velocity distributions of the brightest half of the RV sample (*Gaia* G -band apparent magnitude < 13), one from the faintest half ($G > 13$), and one from *all* stars with RVs. Figure 5 shows the distributions of the faint (blue) and bright (orange)

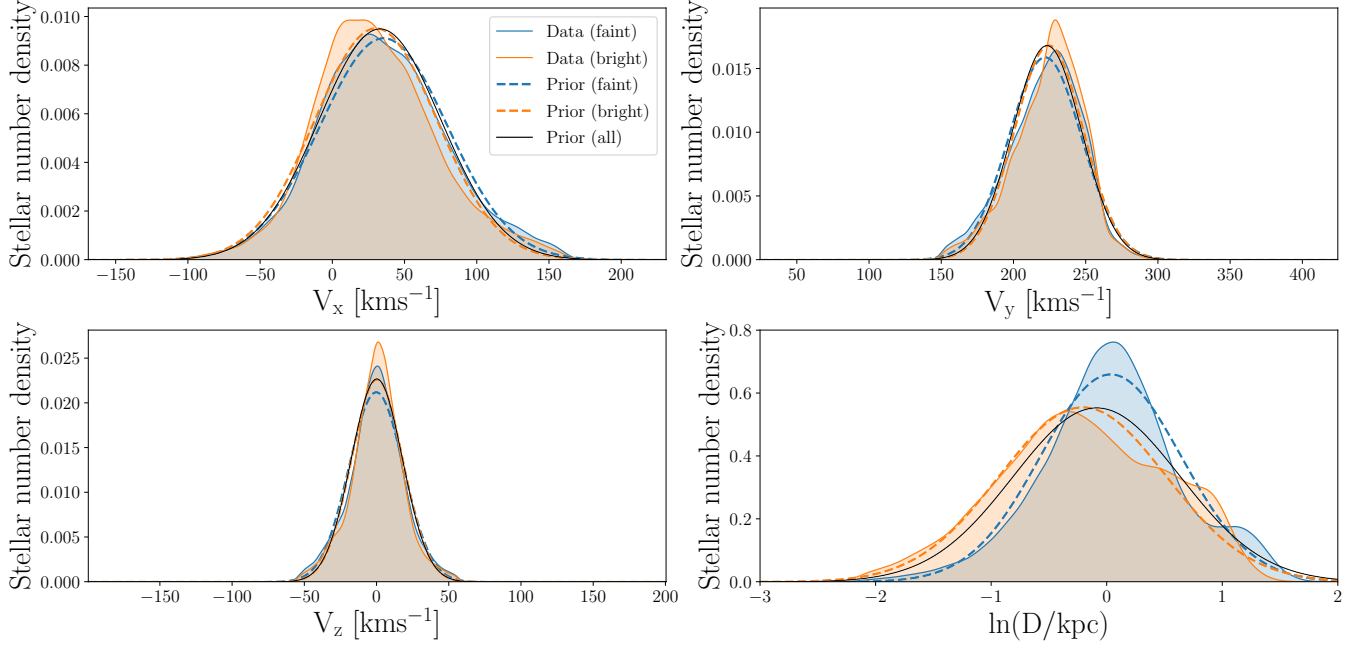
Figure 4. The velocity and distance distributions for stars with RV measurements, used to construct a multivariate Gaussian prior over velocity and distance parameters for stars *without* RVs. The 1- and 2-D distributions of the data are shown in black and the prior is indicated in red.



halves of the RV sample as kernel density estimates (KDEs). The distributions are different because bright stars are typically more massive, younger, more evolved, and/or closer to the Sun on average than faint stars. As a result, these stars occupy slightly different Galactic orbits. The multivariate Gaussian, fit to these distributions, which was used as a prior PDF, is shown as single-dimension projections in figure 5. The Gaussian fit to the bright and faint star distributions are shown as dashed orange and blue lines, respectively. The Gaussian fit to *all* the data, both bright and faint, is shown as a black solid line. The means of the faint and bright distributions differ by 6 kms $^{-1}$, 5 kms $^{-1}$, 1 kms $^{-1}$ and 0.21 kpc, for v_x , v_y , v_z and $\ln(D)$, respectively. The v_x , v_y , and distance distributions of the bright stars are slightly non-Gaussian – more so than the faint stars. This highlights the inadequacy of using a Gaussian distribution as the prior – a Gaussian is only an approximation of the underlying distribution of stars in our sample. As a result of this approximation, inferred velocities that are strongly prior-dependent – (*i.e.* especially those in the \mathbf{y} -direction) may inherit some inaccuracies from the Gaussian prior, which is not a perfect representation of the underlying data. However, given that the populations of stars with and without RV measurements are different, it may be inappropriate to use a more complex, more informative prior anyway.

We inferred the velocities of 1000 stars chosen at random from the RV Kepler sample using each of these three priors and compared the inferred velocity distributions. If the inferred velocities were highly prior-dependent, the resulting

Figure 5. Velocity and distance distributions of faint (blue) and bright (orange) stars with RVs, shown as KDEs. Gaussian fits to these distributions are shown as dashed lines in corresponding colors. The solid black line shows the Gaussian fit to all data (bright and faint combined) and is the prior we ended up using in our model.



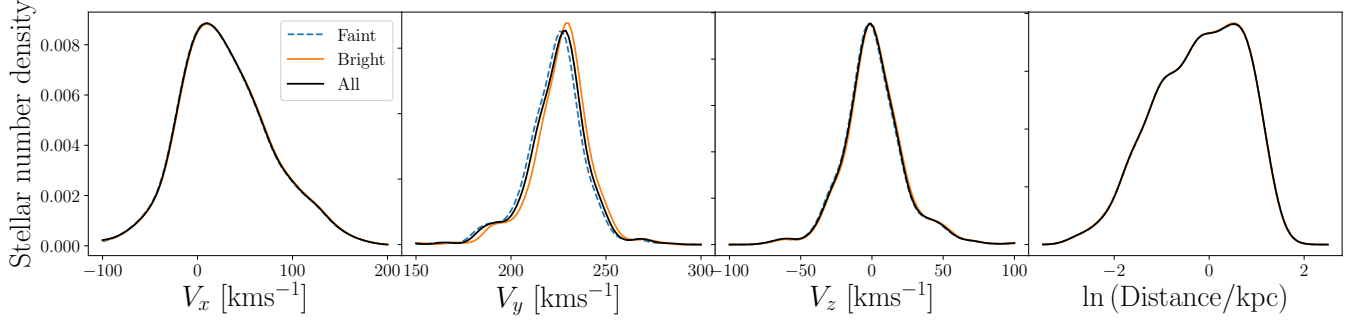
distributions, obtained from different priors, would look very different. The results of this test are shown in figure 6. From left to right, the three panels show the distributions of inferred v_x , v_y , and v_z . The blue dashed line shows a KDE, representing the distributions of velocities inferred using the prior calculated from the faint half of the RV sample. Similarly, the solid orange line shows the distribution of inferred velocities using the prior calculated from the bright half of the RV sample, and the solid black line shows the results of the prior calculated from *all* stars with measured RVs.

The median values of the v_y distributions, resulting from the faint and bright priors, differ by around 4 km s^{-1} . This is similar to the difference in means of the faint and bright populations (5 km s^{-1} , as quoted above). The inferred v_x and v_z distributions differ by 2 km s^{-1} and 0.3 km s^{-1} , respectively. Regardless of the prior choice, the v_x and v_z distributions are similar because velocities in the x and z -directions are not strongly prior dependent: they are tightly constrained with proper motion measurements alone. However, the distribution of inferred v_y velocities *does* depend on the prior. This is because the y -direction is close to the radial direction for Kepler stars (see figure 3), and v_y cannot be tightly constrained without an RV measurement. The distributions of stellar distances are almost identical, irrespective of the prior. This is because distance is very tightly constrained by Gaia parallax and is relatively insensitive to the prior.

Although this test was performed on stars with RV measurements, which are brighter overall than the sample of stars without RVs (*e.g.* figure 1), figure 6 nevertheless shows that v_x and v_z are not strongly prior-dependent. Since this work is chiefly motivated by kinematic age-dating, which mostly requires vertical velocities (v_z) we are satisfied with these results. The difference in the dispersions of v_z velocities, calculated with the three different priors tested above was smaller than 0.5 km s^{-1} . We conclude that the v_x and v_z velocities we infer are relatively insensitive to prior choice, and we adopt a prior calculated from the distributions of all stars with RV measurements (black Gaussians in figure 5). The v_y velocities are more strongly prior dependent and should be used with caution.

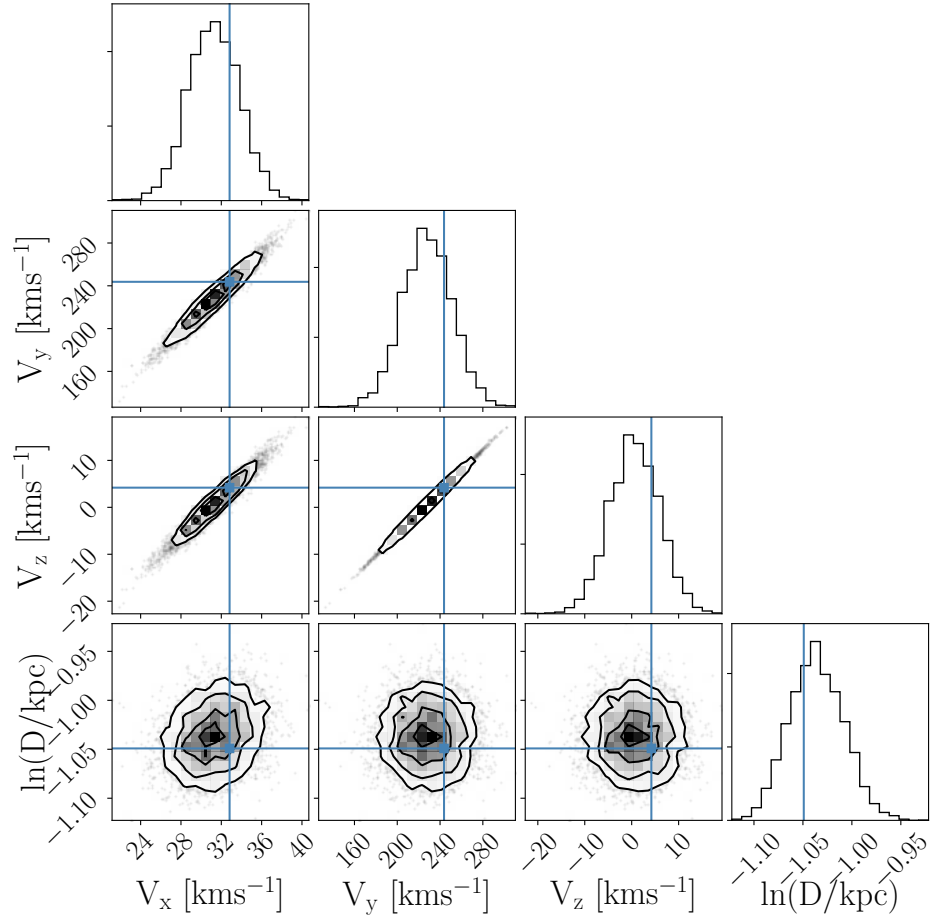
Figure 7 shows the posterior PDF over velocity and distance parameters for a randomly selected Kepler target with an RV measurement, KIC 10350652. Blue lines in each panel indicate the velocities calculated using the RV measurement and the distributions indicated the probability density of the parameters, inferred *without* the RV measurement. The velocity parameters are correlated because the lack of RV introduces a slight degeneracy: the star's proper motion can be equally well described with a range of different velocities. The star's posterior PDF is particularly elongated in

Figure 6. The distributions of velocity and distance parameters, inferred using three different priors. The orange line is a KDE that represents the distribution of parameters inferred with a Gaussian prior, estimated from the bright half of the RV sample ($G < 13$). The blue dashed line shows the results from a prior estimated from the faint half of the RV sample ($G > 13$). The black line shows the results from a prior calculated from all stars with RV measurements and is the prior we adopt in our final analysis.



v_y , which is the velocity most similar to RV. The star's distance is not tightly correlated with its velocity parameters because it is precisely determined by parallax.

Figure 7. The posterior PDF over parameters v_x , v_y , v_z and $\ln(\text{distance})$ for a Kepler target chosen at random: KIC 10350652. This figure shows that the velocity parameters are correlated and the star's posterior is elongated in v_y .



4. RESULTS

4.1. Inferred velocities

In this section we assess the quality of the 3D stellar velocities we infer. Figure 8 shows the distribution of stellar velocities inferred for 5000 randomly selected Kepler stars. The 2D distributions of inferred stellar velocities are plotted in the lower-left panels, with black contours indicating the stellar number density. The red contours in these panels show the marginal projections of the Gaussian prior in 2D. The diagonal panels show the 1D distributions (histograms) of stellar velocities. The black histogram shows the distribution of inferred velocities, the cyan histogram shows the distribution of velocities calculated for stars with RVs (on which the prior was based), and the red lines show the 1D prior distributions. The prior distribution is calculated using the velocities of stars with RVs. If the velocity distributions of stars were Gaussian, the 1D red Gaussians would look like the cyan histograms. In other words, the differences between the red lines and cyan histograms is caused by the non-Gaussianity of the velocity distributions. In each panel, the distribution of inferred velocities is similar to the distribution of directly-measured velocities; the velocities of stars calculated with and without RVs are broadly similar.

There is a slight negative correlation between inferred v_y and v_z velocities, which is visible in the central panel of figure 8. This negative correlation is not seen in the prior, nor is it apparent in the posteriors of individual stars: figure 7 shows that the v_y and v_z parameters are *positively* correlated for KIC 10350652. The negative correlation seen in the population of inferred velocities is caused by the specific orientation of the Kepler field which creates a slight degeneracy between v_y and v_z . This orientation creates a negative correlation in the population of stars, that is not apparent in the posteriors of individual stars. To an observer looking at Kepler field, a star with either a positive v_z or a *negative* v_y would appear to move in the direction of positive v_z , when projected onto the sky. In this sense, v_y and v_z are negatively correlated. However, the observed proper motions of a star without a measured RV could be equally well described by either increasing both v_y and v_z , or decreasing both v_y and v_z . For this reason, the star’s posterior PDF over v_y and v_z will be positively correlated.

To further validate our method, we compare inferred velocities with directly-calculated velocities for stars in our sample with measured RVs. Figure 9 shows the v_x , v_y and v_z velocities, and distances we inferred, compared with those calculated from measured RVs, for 5000 Kepler stars chosen at random. The three velocity components, v_x , v_y and v_z were recovered with differing levels of precision: v_x and v_z are inferred more precisely than v_y . This is because of the position of the Kepler field, shown in figure 3. The velocities of low- v_y stars are underestimated and the velocities of high- v_y stars are overestimated. This is because there is little information to constrain the v_y velocities and the prior pulls the v_y velocities toward the center of the distribution. The v_x , v_y and v_z velocities of stars are correlated, which means that stars with an inaccurate v_y also have slightly accurate v_z and v_x . Despite slight systematic inaccuracies, Around 68% of the inferred velocities are within 1σ of their true velocities; the inferred velocities are consistent with the true velocities.

We provide a table of the directly-calculated, and indirectly-inferred 3D velocities of stars observed by Kepler, in addition to their positional and velocity information from Gaia EDR3, LAMOST DR5 and APOGEE DR16. A description of each column included in that table is provided in table 1.

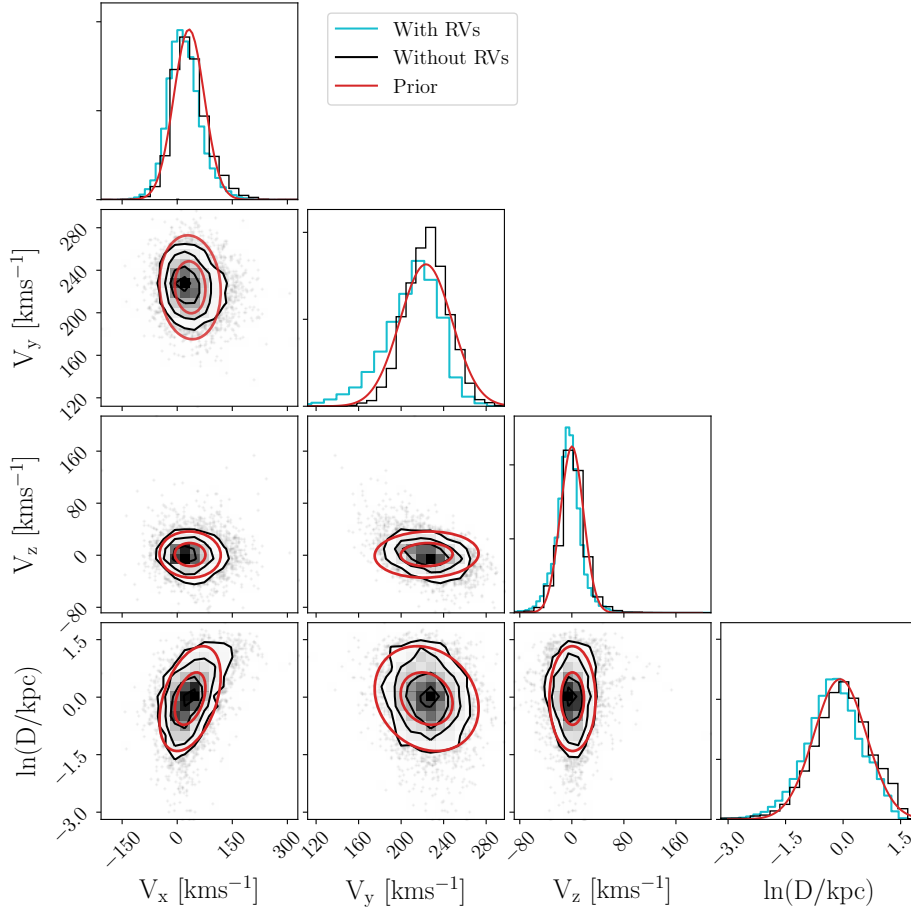
5. CONCLUSION

This paper describes a method for inferring the 3D velocities of stars by marginalizing over missing radial velocity measurements. We focused on stars in the Kepler field because of its potential for studying stellar evolution via kinematic age-dating as well as its advantageous orientation. Located at low Galactic latitude, the Kepler field is almost aligned with the y -axis of the Galactocentric coordinate system. This means that 2D Gaia proper motion measurements alone are sufficient to tightly constrain the v_x and v_z velocities of Kepler stars. Without RV measurements, the v_y velocities of Kepler stars are poorly constrained. However, given that many age-velocity dispersion relations (AVR) are calibrated in *vertical* velocity, v_z is the main parameter of interest for kinematic age-dating and it is precisely constrained by our method: v_z is inferred with a median precision of 4 km s^{-1} .

We compiled kinematic data for Kepler targets from the, Gaia EDR3, LAMOST DR5 and APOGEE DR16 catalogs. Gaia EDR3 provided parallaxes, positions and proper motions for the stars in our sample. Altogether, Gaia DR2, LAMOST DR5, and APOGEE DR16 provided RVs for 58,270 Kepler targets.

We calculated v_x , v_y , and v_z for the 58,270 stars in our sample with RVs using `astropy`. For the remaining stars, we *inferred* v_x , v_y , v_z , and distance while marginalizing over RV. Our prior was a 4D Gaussian in v_x , v_y , v_z and $\ln(\text{distance})$, which was based on the distribution of stars in our sample *with* RVs. Since the populations of stars

Figure 8. The distribution of inferred stellar velocities and distances. Figure 8 shows the inferred velocities of 5000 randomly selected Kepler stars. The 2D distributions of inferred stellar velocities are plotted in the lower-left panels, with black contours indicating the stellar number density. The orange contours in the lower-left panels show the marginal projections of the Gaussian prior distribution in 2D. The upper-right panels in the figure, lying on the plot’s diagonal, show the 1D distributions (histograms) of stellar velocities. The black histogram shows the distribution of inferred velocities, the blue histogram shows the distribution of velocities for stars with RVs, and the orange lines show the 1D marginal Gaussian prior distributions.



with and without RVs in the Kepler field are somewhat different – stars *with* RVs are generally brighter than stars without – we tested the sensitivity of our results to the prior. We split the subsample of stars with measured RVs into two further subgroups: stars brighter and stars fainter than 13th magnitude in Gaia *G*-band (13th being the median magnitude of the Kepler stars with RVs). Priors were constructed from the faint and bright halves of the sample and used to infer the velocities of 1000 stars randomly selected from the total RV sample. Upon examination, we found the final inferred velocities were similar, irrespective of the prior. As expected, v_x and v_z depend very little on the prior but v_y has a stronger prior-dependence because it is difficult to constrain without an RV for Kepler stars. A caveat of our inferred velocities is therefore that the v_y velocities may not be accurate for faint stars in the Kepler field.

Overall, we found that the distribution of inferred velocities for Kepler targets is similar to the velocity distribution of stars with measured RVs. The median precision of inferred v_x , v_y , and v_z velocities is 5, 18, and 4 kms^{-1} respectively. We provide a table of parameters v_x , v_y , v_z , and $\ln(\text{distance})$, with uncertainties and covariances, for a total of 185,223 Kepler targets. This table also contains the positional and velocity information from Gaia DR2, Gaia EDR3, LAMOST DR5, and APOGEE DR16 used in this project.

ACKNOWLEDGEMENTS

This work made use of the `gaia-kepler.fun` crossmatch database created by Megan Bedell.

Figure 9. Velocities calculated with full 6D information compared with velocities inferred without RVs, for 5000 Kepler targets with RV measurements.

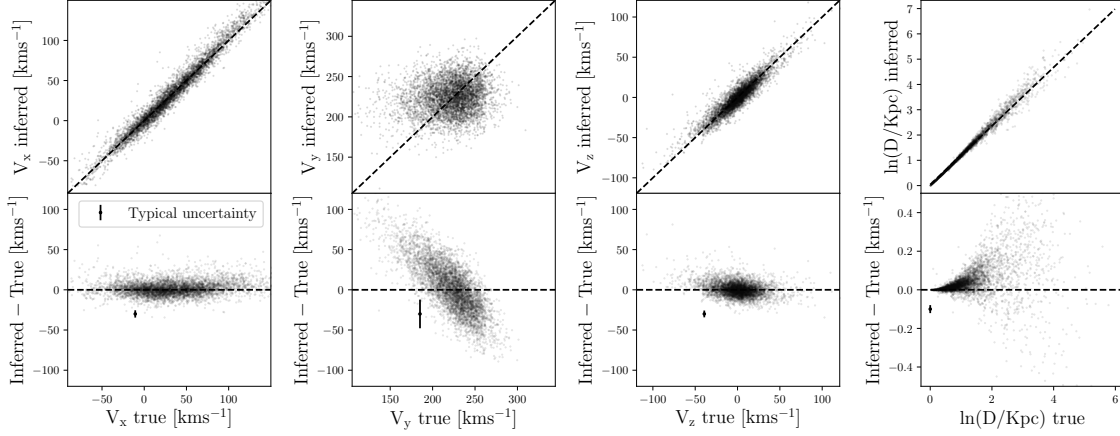


Table 1. The list of columns in the data table published online, which provides the velocities and kinematic information for stars in the Kepler field.

Column name	Description
<code>kic_id</code>	The Kepler Input Catalog ID number of the target.
<code>source_id</code>	The Gaia DR3 ID number of the target.
<code>ra, ra_error</code>	Gaia EDR3 right ascension ($^{\circ}$).
<code>dec, dec_error</code>	Gaia EDR3 declination in degrees ($^{\circ}$).
<code>parallax, parallax_error</code>	Gaia EDR3 parallax (mas).
<code>r_est, r_est_err</code>	Distance (parsec), provided by Bailer-Jones et al. (2021) .
<code>pmra, pmra_error</code>	Gaia EDR3 proper motion in right ascension (mas/yr).
<code>pmdec, pmdec_error</code>	Gaia EDR3 proper motion in declination (mas/yr).
<code>gaia_rv, gaia_rv_error</code>	Gaia DR2 radial velocity (km/s)
<code>apogee_rv, apogee_rv_error</code>	APOGEE DR16 radial velocity (km/s)
<code>lamost_rv, lamost_rv_error</code>	LAMOST DR5 radial velocity (km/s)
<code>vx_calc</code>	The v_x velocity calculated using RV (km/s).
<code>vx_inferred, vx_inferred_error</code>	The median and standard deviation of v_x velocity samples, inferred without RV (km/s).
<code>vy_calc</code>	The v_y velocity calculated using RV (km/s).
<code>vy_inferred, vy_inferred_error</code>	The median and standard deviation of v_y velocity samples, inferred without RV (km/s).
<code>vz_calc</code>	The v_z velocity calculated using RV (km/s).
<code>vz_inferred, vz_inferred_error</code>	The median and standard deviation of v_z velocity samples, inferred without RV (km/s).
<code>vxvy_covar</code>	The covariance between v_x and v_y samples.
<code>vxvz_covar</code>	The covariance between v_x and v_z samples.
<code>vxlnd_covar</code>	The covariance between v_x and $\ln(\text{distance})$ samples.
<code>vyvz_covar</code>	The covariance between v_y and v_z samples.
<code>vylnnd_covar</code>	The covariance between v_y and $\ln(\text{distance})$ samples.
<code>vzlnnd_covar</code>	The covariance between v_z and $\ln(\text{distance})$ samples.

Some of the data presented in this paper were obtained from the Mikulski Archive for Space Telescopes (MAST). STScI is operated by the Association of Universities for Research in Astronomy, Inc., under NASA contract NAS5-26555. Support for MAST for non-HST data is provided by the NASA Office of Space Science via grant NNX09AF08G

and by other grants and contracts. This paper includes data collected by the Kepler mission. Funding for the Kepler mission is provided by the NASA Science Mission directorate.

This work has made use of data from the European Space Agency (ESA) mission *Gaia* (<https://www.cosmos.esa.int/gaia>), processed by the *Gaia* Data Processing and Analysis Consortium (DPAC, <https://www.cosmos.esa.int/web/gaia/dpac/consortium>). Funding for the DPAC has been provided by national institutions, in particular the institutions participating in the *Gaia* Multilateral Agreement.

Software: Astropy (?), Matplotlib (?), Seaborn, etc

REFERENCES

- Ahumada, R., Prieto, C. A., Almeida, A., & *et al.* 2020, ApJS, 249, 3, doi: [10.3847/1538-4365/ab929e](https://doi.org/10.3847/1538-4365/ab929e)
- Angus, R., Aigrain, S., & Foreman-Mackey *et al.*, D. 2015, MNRAS, 450, 1787, doi: [10.1093/mnras/stv423](https://doi.org/10.1093/mnras/stv423)
- Angus, R., Morton, T. D., & Foreman-Mackey *et al.*, D. 2019, AJ, 158, 173, doi: [10.3847/1538-3881/ab3c53](https://doi.org/10.3847/1538-3881/ab3c53)
- Angus, R., Beane, A., Price-Whelan, A. M., et al. 2020, AJ, 160, 90, doi: [10.3847/1538-3881/ab91b2](https://doi.org/10.3847/1538-3881/ab91b2)
- Astropy Collaboration, Robitaille, T. P., & Tollerud *et al.*, E. J. 2013, A&A, 558, A33, doi: [10.1051/0004-6361/201322068](https://doi.org/10.1051/0004-6361/201322068)
- Aumer, M., Binney, J., & Schönrich, R. 2016, MNRAS, 462, 1697, doi: [10.1093/mnras/stw1639](https://doi.org/10.1093/mnras/stw1639)
- Aumer, M., & Binney, J. J. 2009, MNRAS, 397, 1286, doi: [10.1111/j.1365-2966.2009.15053.x](https://doi.org/10.1111/j.1365-2966.2009.15053.x)
- Bailer-Jones, C. A. L. 2015, PASP, 127, 994, doi: [10.1086/683116](https://doi.org/10.1086/683116)
- Bailer-Jones, C. A. L., Rybizki, J., Foesneau, M., Demleitner, M., & Andrae, R. 2021, AJ, 161, 147, doi: [10.3847/1538-3881/abd806](https://doi.org/10.3847/1538-3881/abd806)
- Bailer-Jones, C. A. L., Rybizki, J., & Foesneau *et al.*, M. 2018, AJ, 156, 58, doi: [10.3847/1538-3881/aacb21](https://doi.org/10.3847/1538-3881/aacb21)
- Barnes, S. A. 2003, ApJ, 586, 464, doi: [10.1086/367639](https://doi.org/10.1086/367639)
- . 2007, ApJ, 669, 1167, doi: [10.1086/519295](https://doi.org/10.1086/519295)
- Bird, J. C., Kazantzidis, S., & Weinberg *et al.*, D. H. 2013, ApJ, 773, 43, doi: [10.1088/0004-637X/773/1/43](https://doi.org/10.1088/0004-637X/773/1/43)
- Casagrande, L., Schönrich, R., & Asplund *et al.*, M. 2011, A&A, 530, A138, doi: [10.1051/0004-6361/201016276](https://doi.org/10.1051/0004-6361/201016276)
- Clayton, Z. R., van Saders, J. L., Santos, Â. R. G., et al. 2020, ApJ, 888, 43, doi: [10.3847/1538-4357/ab5c24](https://doi.org/10.3847/1538-4357/ab5c24)
- Cui, X.-Q., Zhao, Y.-H., & Chu *et al.*, Y.-Q. 2012, Research in Astronomy and Astrophysics, 12, 1197, doi: [10.1088/1674-4527/12/9/003](https://doi.org/10.1088/1674-4527/12/9/003)
- Curtis, J. L., Agüeros, M. A., Matt, S. P., et al. 2020, ApJ, 904, 140, doi: [10.3847/1538-4357/abbf58](https://doi.org/10.3847/1538-4357/abbf58)
- Dropulic, A., Ostdiek, B., Chang, L. J., et al. 2021, arXiv e-prints, arXiv:2103.14039, <https://arxiv.org/abs/2103.14039>
- Foreman-Mackey, D., & Barentsen, G. 2019, dfm/exoplanet: exoplanet v0.1.3, v0.1.3, Zenodo, doi: [10.5281/zenodo.2536576](https://doi.org/10.5281/zenodo.2536576)
- Gaia Collaboration, Brown, A. G. A., Vallenari, A., et al. 2020, arXiv e-prints, arXiv:2012.01533, <https://arxiv.org/abs/2012.01533>
- Gaia Collaboration, Brown, A. G. A., Vallenari, A., & Prusti, T. *et al.* 2018, A&A, 616, A1, doi: [10.1051/0004-6361/201833051](https://doi.org/10.1051/0004-6361/201833051)
- Gaia Collaboration, Prusti, T., de Bruijne, J. H. J., & Brown, A. G. A. *et al.* 2016, A&A, 595, A1, doi: [10.1051/0004-6361/201629272](https://doi.org/10.1051/0004-6361/201629272)
- Harris, C. R., Millman, K. J., van der Walt, S. J., et al. 2020, Nature, 585, 357, doi: [10.1038/s41586-020-2649-2](https://doi.org/10.1038/s41586-020-2649-2)
- Holmberg, J., Nordström, B., & Andersen, J. 2007, A&A, 475, 519, doi: [10.1051/0004-6361:20077221](https://doi.org/10.1051/0004-6361:20077221)
- . 2009, A&A, 501, 941, doi: [10.1051/0004-6361/200811191](https://doi.org/10.1051/0004-6361/200811191)
- Lu, Yuxi, Angus, R., et al. 2021, arXiv e-prints, arXiv:2102.01772, <https://arxiv.org/abs/2102.01772>
- Mackereth, J. T., Bovy, J., Leung, H. W., et al. 2019, MNRAS, 489, 176, doi: [10.1093/mnras/stz1521](https://doi.org/10.1093/mnras/stz1521)
- Mamajek, E. E., & Hillenbrand, L. A. 2008, ApJ, 687, 1264, doi: [10.1086/591785](https://doi.org/10.1086/591785)
- Martig, M., Minchev, I., & Flynn, C. 2014, MNRAS, 443, 2452, doi: [10.1093/mnras/stu1322](https://doi.org/10.1093/mnras/stu1322)
- Matt, S. P., MacGregor, K. B., & Pinsonneault *et al.*, M. H. 2012, ApJL, 754, L26, doi: [10.1088/2041-8205/754/2/L26](https://doi.org/10.1088/2041-8205/754/2/L26)
- Metcalf, T. S., & Egeland, R. 2019, ApJ, 871, 39, doi: [10.3847/1538-4357/aaf575](https://doi.org/10.3847/1538-4357/aaf575)
- Nordström, B., Mayor, M., & Andersen *et al.*, J. 2004, A&A, 418, 989, doi: [10.1051/0004-6361:20035959](https://doi.org/10.1051/0004-6361:20035959)
- Oh, S., Price-Whelan, A. M., Hogg, D. W., Morton, T. D., & Spergel, D. N. 2017, AJ, 153, 257, doi: [10.3847/1538-3881/aa6ffd](https://doi.org/10.3847/1538-3881/aa6ffd)
- Price-Whelan, A. M., Sipőcz, B. M., & Günther *et al.*, H. M. 2018, AJ, 156, 123, doi: [10.3847/1538-3881/aabc4f](https://doi.org/10.3847/1538-3881/aabc4f)
- Salvatier, J., Wiecki, T. V., & Fonnesbeck, C. 2016, PyMC3: Python probabilistic programming framework, <http://ascl.net/1610.016>

- Skumanich, A. 1972, ApJ, 171, 565, doi: [10.1086/151310](https://doi.org/10.1086/151310)
- Soderblom, D. R. 2010, ARA&A, 48, 581,
doi: [10.1146/annurev-astro-081309-130806](https://doi.org/10.1146/annurev-astro-081309-130806)
- Spada, F., & Lanzafame, A. C. 2019, arXiv e-prints,
arXiv:1908.00345. <https://arxiv.org/abs/1908.00345>
- Stark, A. A., & Brand, J. 1989, ApJ, 339, 763,
doi: [10.1086/167334](https://doi.org/10.1086/167334)
- Stark, A. A., & Lee, Y. 2005, ApJL, 619, L159,
doi: [10.1086/427936](https://doi.org/10.1086/427936)
- Strömberg, G. 1946, ApJ, 104, 12, doi: [10.1086/144830](https://doi.org/10.1086/144830)
- The Theano Development Team, Al-Rfou, R., Alain, G.,
et al. 2016, arXiv e-prints, arXiv:1605.02688.
<https://arxiv.org/abs/1605.02688>
- Ting, Y.-S., & Rix, H.-W. 2019, ApJ, 878, 21,
doi: [10.3847/1538-4357/ab1ea5](https://doi.org/10.3847/1538-4357/ab1ea5)
- van Saders, J. L., Ceillier, T., & Metcalfe *et al*, T. S. 2016,
Nature, 529, 181, doi: [10.1038/nature16168](https://doi.org/10.1038/nature16168)
- van Saders, J. L., Pinsonneault, M. H., & Barbieri, M.
2018, ArXiv e-prints. <https://arxiv.org/abs/1803.04971>
- Wielen, R. 1977, A&A, 60, 263
- Xiang, M., Ting, Y.-S., & Rix *et al.*, H.-W. 2019, ApJS,
245, 34, doi: [10.3847/1538-4365/ab5364](https://doi.org/10.3847/1538-4365/ab5364)
- Yu, J., & Liu, C. 2018, MNRAS, 475, 1093,
doi: [10.1093/mnras/stx3204](https://doi.org/10.1093/mnras/stx3204)